

Single filament electrophoresis of F-actin and filamentous virus fd

Guanglai Li, Qi Wen, and Jay X. Tang

Physics Department, Brown University, Providence, Rhode Island 02912

(Received 20 October 2004; accepted 21 December 2004; published online 10 March 2005)

We have developed an electrophoretic cell suitable for single-molecule electrophoresis. The setup works for fluorescently labeled macromolecules by direct recording of their motion under an external electric field. The electrophoretic mobility of rodlike, polydisperse actin filaments (F-actin) were measured, as well as its dependence on the orientation of the filaments. A dipping effect is observed and quantitatively accounted for by the difference in hydrodynamic drag between motions along and perpendicular to the long axis of a filament. When averaged over all orientations, the mobility of F-actin in 50 mM KCl and 2 mM MgCl₂ is determined to be $-(8.5 \pm 0.7) \times 10^{-5} \text{ cm}^2/(\text{V s})$. This method is also used to compare the mobility of F-actin and fd virus in a mixture of them. A reliable ratio of 1.26 is measured for fd virus to F-actin. The influence of the orientation dependent drag on electrophoretic mobility is discussed and a strategy for reliable measurement is proposed. © 2005 American Institute of Physics. [DOI: 10.1063/1.1859284]

I. INTRODUCTION

Electrophoresis is a widely used technique for studies of charge related properties of polymers, colloids, and biomolecules in particular, such as proteins, DNA, and RNA. The conventional technique typically uses a gel matrix such as agarose and polyacrylamide. The electrophoretic mobility measured is strongly affected by the mesh size of the gel, thus the technique is most appropriate for size characterization and separation.¹ Since confining the sample in a thin capillary retards convection and undesirable mixing, capillary electrophoresis has been applied, either with or without gel matrix. With the development of coated capillaries to reduce or eliminate the electro-osmotic flow (EOF), capillary electrophoresis has become quite suitable for the measurement of free solution mobility, using a small amount of sample.^{2,3} Capillary electrophoresis can also be performed in microfabricated channels. Application of multiple microchannels as miniaturized capillaries increases the efficiency of the measurements.⁴

In a free solution, electrophoretic mobility is proportional to the total effective charge and inversely proportional to the hydrodynamic friction.⁵ In a typical measurement, the average speed of an assembly of molecules under an electric field is measured and the mobility is the ratio of the average speed to the electric field. The widely used commercial instruments measure the mobility of charged particles either by dynamic light scattering or by detecting the laser Doppler effect, such as DELSA 440 (Beckman-Coulter, Inc).⁶ A typical measurement using a commercial instrument requires ≈ 1 ml sample, and the measured mobility is the average of an ensemble of charged particles.

Recently, single-molecule electrophoresis is developed to measure free-solution mobility of individual molecules. In Castro's method,^{7,8} a moving molecule under an electric field passes through two laser beams over a short distance and emits bursts of fluorescence. The time between the two successive bursts is measured and used to calculate the mobility.

In Yeung's method,^{9,10} the motion of individual fluorescently labeled molecules under an electric field is recorded by fluorescence microscopy and the speed of each molecule is measured. This method is capable of measuring mobility of molecules in a sample that contains molecules with various sizes or even different species. Therefore, the technique is applicable to biomolecules that are difficult for isolation and purification. It is even possible to measure the mobility of molecules within a living cell.

However, on the single-molecule level, translational and rotational Brownian motions¹¹ fundamentally affect the measurements. Specifically, translational Brownian motion adds uncertainty to the travel distance, which can cause large errors if both the speed of the molecules and their travel distance are small. The drift speed of a nonspherical molecule is related to its orientation, so the instant speed changes due to rotational Brownian motion, as well. Many biomacromolecules are rodlike, such as short DNA fragments,¹² actin filaments,¹³ and microtubules.¹⁴ The drag coefficient of their motion in fluid strongly depends on the orientation. Therefore, in a single-molecule electrophoresis measurement, effects of rotational Brownian motion must be considered.

In this paper, we study the electrophoresis of F-actin and filamentous virus fd by tracking the motion of individual filaments using fluorescence microscopy. The effect of orientation on mobility is measured. We also show that the technique can be usefully applied to characterization of various macromolecular species in a mixture, as well as various particles of one species with variable charge densities.

II. EXPERIMENTS

A. Preparation of F-actin and fd virus

F-actin was polymerized from the globular monomers G-actin by adding 50 mM KCl and 2 mM MgCl₂ into the protein solution initially containing 0.2 mM CaCl₂, 0.5 mM ATP, 0.5 mM DTT, and 2.0 mM Tris-HCl buffer, pH 7.95 at room temperature. A solution containing the same concentra-

tions of all the ions listed is referred to as F-buffer, which is used to dilute F-actin. F-actin was labeled at a molar ratio of 1:1 with rhodamine (TRITC-) or fluorescein (FITC-) phalloidin (Sigma, St Louis, MO). Before making a sample for fluorescence microscopy, a stock solution of 0.4 mg/ml F-actin was diluted using F-buffer to 1 $\mu\text{g}/\text{ml}$. In order to reduce the effect of photobleaching, an antibleaching protocol was followed, so that the F-buffer used for dilution has been previously added 20 $\mu\text{g}/\text{ml}$ catalase, 0.5 mg/ml glucose, 0.1 mg/ml glucose oxidase, and 0.25 vol % mercaptoethanol. Selected control experiments were also performed without antibleaching reagents to ensure that the measured electrophoretic mobility values were not affected by them.

Bacteriophage fd was prepared following a standard procedure.¹⁵ *E. coli* K-38 cells were infected with fd and grown for 10 h in Luria-Bertani (LB) medium. The culture was then centrifuged at 9950 g (7500 RPM using a BECKMAN JA-10 rotor) for 30 min at 4 °C to remove the bacteria. The supernatant was added with 0.5 M NaCl and 4 wt % polyethylene glycol (PEG 8000), stirred for 1 h, and then centrifuged at 9950 g for 45 min at 4 °C. The pellet was resuspended in a virus buffer containing 100 mM NaCl and 10 mM Tris-Cl, pH=8.0, and further purified through a CsCl density gradient ultracentrifugation step, followed by extensive dialysis against a 5 mM Imidazole buffer, pH=7.0. Concentration of fd viruses was determined by measuring absorbance

at 269 nm using UV spectrophotometer (SHIMADZU UV-1601) with an extinction coefficient $\epsilon = 3.84 \pm 0.06 \text{ mg}^{-1} \text{ cm}^2$. The fd viruses in the imidazole buffer were labeled by rhodamine succinimidyl ester, following a procedure described previously.¹⁶ There are ≈ 2700 copies of coat protein on the virus surface. The fraction of the virus coat protein labeled was $\approx 1:10$.

The concentrated fd virus was diluted in F-buffer and then mixed with FITC-labeled F-actin. The concentrations of fd and F-actin in the mixture were 1.0 $\mu\text{g}/\text{ml}$ and 0.8 $\mu\text{g}/\text{ml}$, respectively.

B. Atomic force microscope imaging

Atomic force microscope (AFM) imaging was used to characterize the coverage and uniformity of the coating of the glass slides and coverslips, which were later used to build the sample cells. All images were obtained using a Nanoscope IIIa Dimension 3100 (Digital Instruments, Veeco Metrology, Santa Barbara, CA) using the contact mode in air.

C. Surface treatments of sample slides

Polyvinyl alcohol (PVA) coating of capillary tubes is shown to greatly reduce the EOF in capillary electrophoresis measurements to less than 10% of that of uncoated tubes.¹⁷⁻¹⁹ Here we used PVA to coat glass slide and coverslip surfaces. A cleaning procedure was performed before PVA coating by which the glass slides and coverslips were immersed in a solution of 6 g Nochromix (GODAX Laboratories, Inc.) in 100 ml concentrated H_2SO_4 for 1 h and then rinsed thoroughly with water. The cleaned glass slides and coverslips were vertically immersed in 0.3% PVA (Poly-

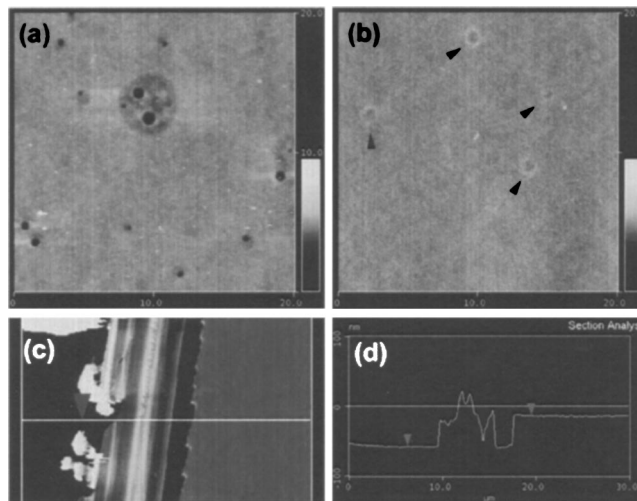


FIG. 1. AFM images of PVA coatings on glass slides. (a) Following a single coating and heating treatment, several holes are noted on the coating in a $20 \times 20 \mu\text{m}^2$ area. (b) After a double coating and heating process, arrows indicate that all the holes have been filled. (c) Double coating partly scratched off. (d) A line scan as indicated in (c) reveals the thickness of the coating to be ~ 50 nm.

sciences, Inc, MW 78 000) solution. The solution was pumped out slowly so that the liquid surface went down at 6 mm/min, leaving a thin layer of coating on the glass surface. The coated glasses were then heated at 150 °C for 2 h.

The quality of coating was examined by AFM in contact mode, as shown in Fig. 1(a). We noted the formation of holes in the coating, which were typically on the order of 1 μm in diameter. Preparations over several sets of slides were made to avoid the formation of these holes, but unsuccessfully. To fill these holes, we repeated the coating and heating process over each set of slides, which resulted in total coverage of the coating. One representative set of images were shown in Fig. 1 to demonstrate the effect of repeated coating. Arrows show a few holes formed in the first coating [Fig. 1(a)], all of which were filled in the second coating [Fig. 1(b)]. The root mean square roughness of the surface is ≈ 0.4 nm. To measure the thickness of the coating, the coated surface was scratched with a needle and imaged with AFM across the scratch. This simple method appeared to work well since the glass surface was found to be much more scratch resistant than the PVA coating. Otherwise, one would expect rather rough surface features after scratching due to the manual operation, which was expected to be uneven no matter how gentle it was applied. As shown in Fig. 1(c), the coating on the left side was mostly removed, while the exposed glass surface remained flat, as well. Fig. 1(d) is the cross section along the white line in Fig. 1(c) and the thickness of the coating was detected to be ≈ 50 nm.

The effect of PVA coating was compared with a more commonly used surface treatment, namely, the coating of glass surface with an inert protein such as bovine serum albumin (BSA). For BSA coating, the glass slides and coverslips were cleaned under the same procedure above, followed by incubating the glass slides and coverslips in 1mg/ml BSA in F-buffer for over 30 min. The slides and cover slips were then thoroughly rinsed with de-ionized buffer, and then ei-

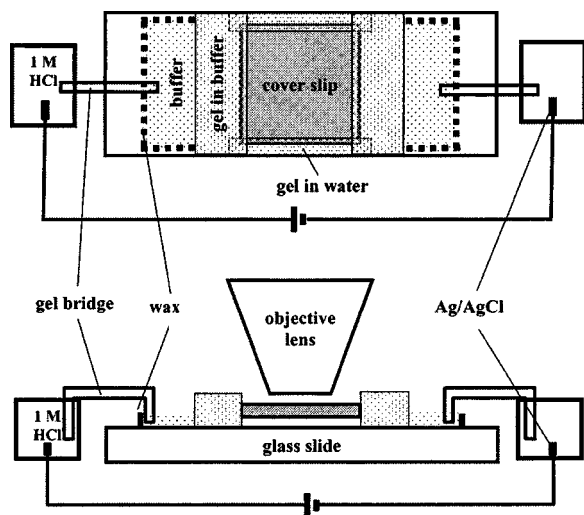


FIG. 2. Top view and side view of the setup for electrophoresis and fluorescence microscopy.

ther dried before use, or rinsed with F-buffer and applied with a drop of the sample without letting the surface dry. No significant difference was noted between the BSA treatments with and without drying in the final step.

D. Electrophoresis setup

Figure 2 depicts the experimental setup for electrophoresis. Here is a brief procedure to assemble such a device. First, a drop of $50 \mu\text{l}$ solution is added on a glass slide and then covered with a cover slip, both having been coated as described above. Excess solution is removed with filter paper quickly after the cover slip is pressed against the slide. The thickness of the sample is conveniently controlled at this stage by the pressing force. Two opposite sides of the slide sample are sealed with agarose gel made from 3.0 wt % agarose (Sigma, A4804) in de-ionized water. The agarose purchased from Sigma is described as having “not detectable” electroendosmosis. Within a couple of minutes after poured out of a warm solution (50°C), the thin agarose stripes gel. Next, the two ends are sealed with the same agarose gel at 3.0 wt %, but prepared in F-buffer. Drops of F-buffer are then added to connect the gels at the ends of the coverslips to two previously placed small tubes, each containing the same agarose gel formed in F-buffer. The tubes act as electrical bridges between the sample chamber and two small reservoirs of 1M HCl each containing Ag wire to serve as electrodes. In this setup, the Ag/AgCl reaction at the electrodes can take place reversibly while HCl is prevented from entering the sample for over several minutes in the applied field up to 1000 V/m . A Nikon Eclipse E800 epifluorescence microscope with a $100\times$ oil immersion objective lens was used for fluorescence imaging. The images were acquired at 10 or 20 frames per second using a CoolSnap Cooled charge-coupled device camera (Roper Scientific, NJ). Video segments of moving actin filaments were analyzed using the Metamorph software (Universal Imaging, IN).

The strength of local electric field near a polyelectrolyte surface is typically on the order of 10^5 V/cm , estimated based on an electrostatic energy on the order of

$k_B T$ (25 meV) and a Debye screening length on the order of 1 nm at an ionic strength around 100 mM. It is reasonable to expect the electrophoretic mobility to vary dependent on the field strength once the counterion distribution within the shear layer is affected. However, since the actual applied field in our experiment is weaker by four orders of magnitude, the average speed of F-actin is found to be proportional to the field strength.

E. Data collection

For thin samples with thickness around one micrometer,²⁰ which is less than the depth of focus, the filaments remain in focal plane during observation and are tracked in the full field of view. For thicker samples, the filaments tend to move away from the focal plane. We only track F-actins and fd viruses that are visible in the field of view for more than 3 s and 1 s, respectively. Under a given electric field, the speed of a filament along the electric force, opposite to the direction of electric field, is obtained by measuring the moving distance during the tracking time. The average speed of filaments under particular field strength is obtained by averaging over the speed along the electric force direction of 16 randomly selected filaments.

III. RESULTS AND ANALYSIS

A. Suppression of electro-osmotic flow by PVA coating

To show the effect of PVA coating on reducing EOF, the speed profile of FITC labeled F-actin in thick samples made from BSA coated and PVA coated glasses were compared. A series of movies were taken when the focal plane was paused at different distances from the bottom surface to the top, by incrementally turning the focusing knob of the microscope. The average speed of F-actin was then determined at each focal plane. The results are shown in Fig. 3 for samples in both PVA and BSA coated cells. For BSA coated sample, the speed is larger at center and markedly smaller close to glass surfaces, showing a parabolic profile [Fig. 3(a)]. The profile is explained below.

BSA coated surface is negatively charged. It generates an EOF along electric field by positive counter ions close to the surface. In an open chamber, the effect will cause a plug flow. In our experiment, however, since the chamber is sealed by the gel, there is no net flow across the cross section of the chamber. Therefore, the EOF generated by the surface will cause a return flow in the opposite direction to that of the electric field in the central layer. F-actin filaments are negatively charged and thus move in the opposite direction to that of electric field in the absence of a flow field. Therefore, the total effect is that the filaments move faster at the center than close to the walls as a result of vectorial addition.

Figure 3(b) shows the speed profile of a PVA coated sample. The results show marked difference from a BSA coated sample. Except for those very close to the surfaces, there is little variation in the measured speed in the PVA coated sample. The slightly lower speed close to surface may

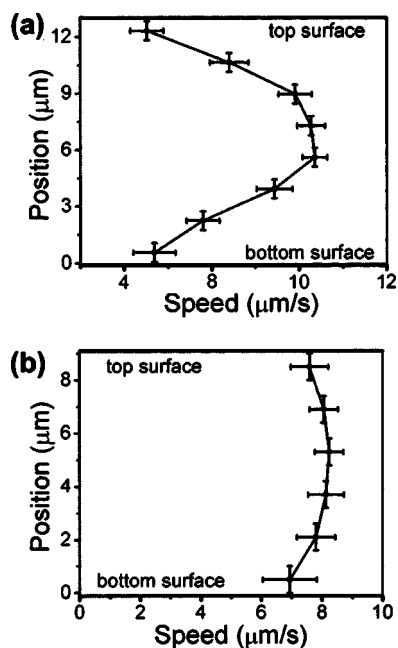


FIG. 3. Speed profile of samples confined in BSA (a) and PVA (b) coated slides and cover slips. The drift speeds were measured from video segments taken at the focal plane at various distances from the bottom surface. The standard errors for both position and speed are indicated.

be due to the larger drag force on F-actin by the wall.^{14,20} These results indicate that the PVA coating greatly reduces the EOF.

The stability of speed with time is also tested by measuring the average speed of F-actin at different times after the voltage is applied. The speed at time t is averaged over 16 randomly selected filaments within the time window of $(t-0.25)$ s to $(t+0.25)$ s. As shown in Fig. 4, the speed does not vary with time within the error of detection. Thus, in principle, the average speed can be measured at any time after applying a voltage. In practice, all data in this study were acquired within a few minutes after the application of electric field in order to keep the electrochemical complication at the minimum.

B. Orientation dependence of moving speed under electric field

The direct recording gives rise to a visual account of how fluorescently labeled F-actin moves under an electric

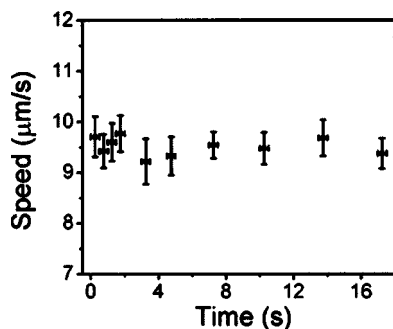


FIG. 4. Average speed of F-actins does not change with time after the voltage is applied. Error bars indicate standard errors obtained by averaging values over 16 filaments.

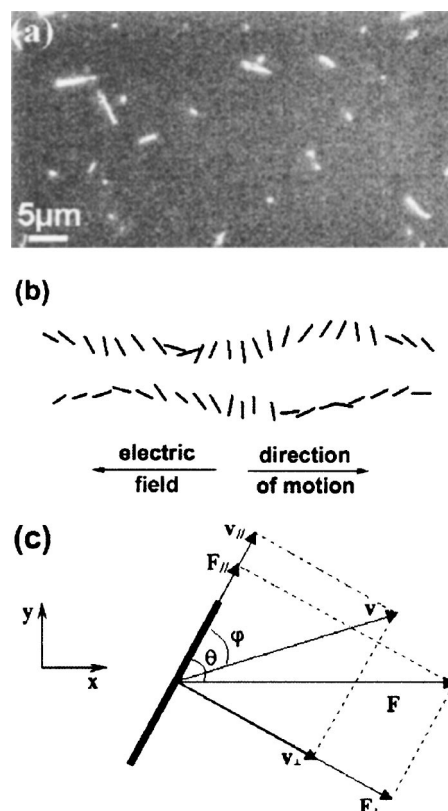


FIG. 5. (a) A fluorescence image of TRITC labeled F-actin in a thin sample showing all actin filaments in the view field. (b) Trajectories of two $3.3 \mu\text{m}$ long filaments moving from left to right by superimposing the position every 0.2 s. (c) Force analysis of F-actin under electric field. The electric field is opposite to the moving direction as indicated in (b).

field. In order to track individual filaments over a long time, thin samples are used. The thickness of a typical sample is less than the depth of focus of the $100\times$ objective so that all labeled filaments can be observed clearly at all times, as shown in Fig. 5(a). One feature of a rodlike molecule moving in an unbounded liquid is the anisotropy in drag coefficients along and perpendicular to the rod axis.^{21–23} This anisotropy has been noted for F-actin when the filaments undergo Brownian motion as they are confined between two walls.²⁰ In the electrophoresis experiment, we observe an interesting phenomenon noted as the “dipping effect,” as shown in Fig. 5(b) for two $3.3 \mu\text{m}$ long F-actin at 0.2 s intervals. When tilted away from their migration direction, the filaments appear to either “dive down” or “shoot up” along the orientation of their long axis. This effect is expected for a rod moving in a viscous medium since the electrophoretic mobility is a second rank tensor relating the velocity and electric field vectors. The observed dipping effect is analyzed in detail below.

When a rod makes an angle with a driving force in a viscous medium, it not only moves in the direction of force, but also has a velocity component perpendicular to the force [Fig. 5(c)]. While all F-actin undergoes directed motions driven by the electric field, its orientation frequently varies, characteristic of the rotational Brownian motion. Note that since F-actin has a uniform linear charge density, no torque is exerted on the filament when the applied electric field is uniform. Since the drag coefficient for the filament moving

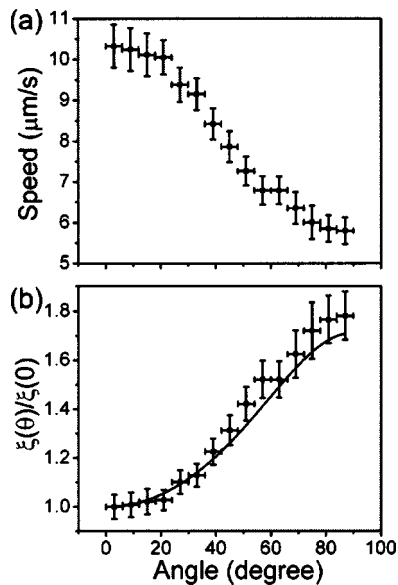


FIG. 6. Speed of F-actin along electric force (a) and relative drag coefficient (b) as a function of angle between F-actin and the direction of the electric force. Data are binned every 6° . Standard errors are shown. Solid line in (b) is calculated from Eq. (4).

perpendicular to its axis is almost twice that moving along its axis, the filament tends to drift along the direction of its axis, noticeable whenever the orientation deviates from the direction of the applied field. The result is the observed dipping effect. Clearly, the direction of motion changes with the filament orientation.

The orientation dependence of average speed along electric force can be measured for F-actin. Mass center positions and angles between consecutive traces with the presence of constant electric force are measured at 0.05 s time interval in the same field of view of a thin sample. For a $3 \mu\text{m}$ long F-actin, the difference in angle between two positions is typically less than 10° within the 0.05 s interval. Thus the orientation of the filament during the time interval can be approximated by the average angle between the initial and final orientations. The speed along the electric force at this orientation is approximated by the average speed along the electric force between two consecutive positions. The velocity and angle of 40 actin filaments with lengths between 3.0 and $4.0 \mu\text{m}$ were measured. The velocity values were averaged over all filaments spanning every 6° in orientation in order to remove the uncertainty introduced by the translational Brownian motion. We prove later that the field driven velocity depends on length only weakly, as $\ln(L/d)$. The spread in length thus contributes less than 5% error to the average velocity, which was neglected. The measured velocity as a function of orientation is shown in Fig. 6(a).

We define the drag coefficient $\xi(\theta)$ of a filament having an angle θ with electric force as $\xi(\theta) = F/V_E(\theta)$, where F is the electric force on the filament and $V_E(\theta)$ the speed along the electric force. The drag coefficient $\xi(\theta)$ is normalized with $\xi(3^\circ)$, the drag coefficient of the rod nearly parallel to the electric force, and the result is plotted in Fig. 6(b). For simplicity, we assume $\xi(0^\circ) = \xi(3^\circ)$ since $V_E(\theta)$ varies little with θ when the angle is close to 0, as shown in Fig. 6(a).

The above observation can be analyzed in terms of the anisotropy of drag coefficients of a rod. For a rod in a bulk solution, drag coefficients along and perpendicular to its axis are

$$\xi_{\parallel} = \frac{2\pi\eta L}{[\ln(L/d) + \gamma_{\parallel}]}, \quad (1)$$

$$\xi_{\perp} = \frac{4\pi\eta L}{[\ln(L/d) + \gamma_{\perp}]}, \quad (2)$$

where η is solvent viscosity,²⁰ L and d are the length and diameter of the rod, and the values of two correction parameters are $\gamma_{\parallel} = -0.114$ and $\gamma_{\perp} = 0.886$.²¹

Since two different drag coefficients apply to the two velocity components of F-actin, projection of the velocity vector in the direction along the electric field is as follows:

$$V_E(\theta) = \frac{E\sigma}{4\pi\eta} \{ 2[\ln(L/d) + \gamma_{\parallel}] \cos^2 \theta + [\ln(L/d) + \gamma_{\perp}] \sin^2 \theta \}, \quad (3)$$

where E is the electric field, σ is the effective linear charge density along F-actin, and θ is the angle between F-actin axis and the direction of the electric force. $V_E(\theta)$ only weakly depends on filament length in proportion to $\ln(L/d)$.

The normalized drag coefficient as a function of orientation is

$$\xi(\theta)/\xi(0^\circ) = \frac{2[\ln(L/d) + \gamma_{\parallel}]}{2[\ln(L/d) + \gamma_{\parallel}] \cos^2 \theta + [\ln(L/d) + \gamma_{\perp}] \sin^2 \theta}. \quad (4)$$

This equation is plotted in Fig. 6(b) and compared with the measured orientation dependence. The measured orientation dependence of drag coefficient agrees with Eq. (4) within the experimental error.

C. Mobility measurement

Using the same setup, we can measure the mobility of various fluorescently labeled macromolecules. To measure the mobility, the strength of electric field must be determined. One might assume that the electric field is trivially determined by dividing the applied voltage by the width of the coverslip, over which the electric current flows. This is, however, not valid for thin samples. The coverslip is $22 \times 22 \text{ mm}^2$ in size. For a sample of thickness only on the order of $1 \mu\text{m}$, the variation in thickness over the entire area tends to be relatively large, hence the electric field is rather inhomogeneous. At a given applied voltage, the measured speed will be different at different positions. This variation is reduced in a thicker sample. If the coverslip is parallel to the glass slide, the electric field in the sample will be V/d , the ratio of voltage drop over the width of the coverslip. However, this condition was not guaranteed for every sample. Fortunately, as long as both the coverslip and the slide surfaces are flat, the electric field at the center of the coverslip is always V/d , even if there is some tilt between the coverslip and glass slide. As shown in Fig. 7, three sets of speed at various voltage values measured at the center of the cover-

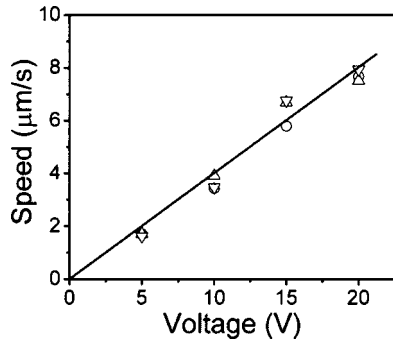


FIG. 7. Linear relationship between the average speed of F-actin and the applied voltage. Fits to measurements at the center of the cover slip of three different samples give almost the same mobility.

slip from three different samples yield approximately the same mobility, with an averaged value of $-(8.5 \pm 0.7) \times 10^{-5} \text{ cm}^2/(\text{V s})$. (see Fig. 7). The data in Fig. 7 also confirms that the measured electrophoretic mobility is independent of the strength of the electric field in the range applied in our experimental setup.

The setup can compare the mobility of the same or different molecules labeled with different dyes in the same buffer conditions. For a sample mixture of FITC labeled F-actin and rhodamine labeled fd virus, a first movie was taken for FITC F-actin for 20 s using a fluorescein filter, and then the filter was switched to rhodamine to take a second movie for rhodamine labeled fd virus for 20 s at the same location of the sample and under the same electric field. The speeds were measured from the movies. Table I shows the results for FITC labeled F-actin and rhodamine labeled fd virus from thick or thin samples at various voltage values and positions. As discussed above, the speed values vary at different measurements, but the ratio of speeds of virus to that of F-actin remains constant among all the measurements. The average value of this ratio is 1.26. Based on this ratio and the F-actin mobility of $-(8.5 \pm 0.7) \times 10^{-5} \text{ cm}^2/(\text{V s})$, the mobility of fd is obtained to be $-(1.07 \pm 0.09) \times 10^{-4} \text{ cm}^2/(\text{V s})$ under the ionic condition of F-buffer. This value for fd is comparable to what determined in a separate recent study,¹⁶ although the previous measurements of fd mobility was not performed in the F-buffer condition. Nevertheless, the comparison above shows that if the mobility of

TABLE I. Speeds of virus (V_{virus}) and F-actin ($V_{\text{F-actin}}$) at different positions and in different samples, measured at two values of electric field. The ratio of speeds between fd virus and F-actin remains nearly constant.

Sample	Position	Voltage		$V_{\text{F-actin}}$	V_{virus}	$V_{\text{virus}}/V_{\text{F-actin}}$
		(V)	(V)			
1, thick	1	20	8.0	10.3	1.29	
2, thick	1	20	8.1	10.1	1.24	
3, thin	1	20	13.8	17.5	1.27	
	2	20	11.7	14.5	1.24	
4, thin	1	10	5.1	6.4	1.26	
	2	10	7.7	9.6	1.25	

one molecule is known, another one can be determined reliably according to the ratio measured through the technique introduced in this study.

We also measured the speed of TRITC- and FITC-phalloidin labeled F-actin in a mixture of them. No difference in their speeds was detected. Phalloidin is a mushroom toxin of molecular weight about two orders of magnitude smaller than each actin protomer, and the specific binding of phalloidin to F-actin does not change its conformation or drag coefficient. According to the description of the compounds in the product handbook by Molecular Probes (Eugene, Oregon), both phalloidin and the two fluorescently conjugated forms used in this study carry no net charge at neutral pH. Therefore, possible effects on the hydrodynamic properties or electrophoretic motility are negligible, if at all. Our experimental finding of the same electrophoretic mobility between actin filaments labeled with the two different dyes is indeed consistent with the known properties of the probes used.

IV. DISCUSSION

The drift speed of a protein filament in an electric field depends on its orientation, i.e., the angle between the filament and the direction of the electric force on it (the reverse direction of the electric field). This dependence is described by Eq. (3). Due to rotational diffusion, the filament constantly changes its orientation, hence the instant speed. In the experiment, we can only track a filament for a limited period of time T . During this time the filament moves a distance L along the direction of electric force, and the speed of the filament is L/T . The speed depends on the time interval of this period and the angle when the recording is started, which is referred below as the starting angle.

The probability for a filament to change its orientation from θ at time t to θ' at time t' through rotational diffusion is

$$P(\theta, t | \theta', t') = \frac{1}{\sqrt{2\pi D_r(t' - t)}} e^{-(\theta' - \theta)^2 / 2D_r(t' - t)}, \quad (5)$$

where D_r is the rotational diffusion constant.²⁴

To study the effect of rotational diffusion on the speed measurement, computer simulations were performed to obtain the speed and standard deviation of a filament under the electric field over a time interval T , which was equally divided into N steps, noted as $t_0, t_1, t_2, \dots, t_{N-1}$, respectively. In the simulations, the step size $\Delta t = t_n - t_{n-1} = 0.001 \text{ s}$ was fixed, and N was determined by T as $N = T/\Delta t$. The angle between the filament orientation and the direction of electric force on the filament is determined as follows: choose an angle θ_0 at t_0 , and then randomly select angles for the following moments according to Eq. (5):

$$P(\theta_n, t_n | \theta_{n+1}, t_{n+1}) = \frac{1}{\sqrt{2\pi D_r \Delta t}} e^{-(\theta_n - \theta_{n+1})^2 / 2D_r \Delta t}.$$

Using Eq. (3), we calculate $V_E(t_n)$ at $t = t_n$ and take it as the speed of the filament between t_n and t_{n+1} . The speed during time interval T is $V = (1/N) \sum_{n=0}^{N-1} V_E(t_n)$. Due to the stochastic nature of the rotational diffusion, repeating the same process

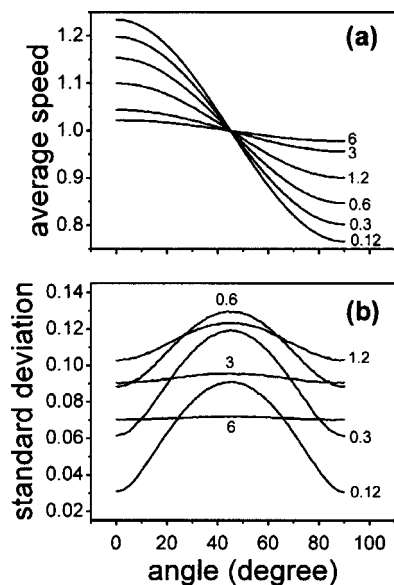


FIG. 8. Average speed (a) and standard deviation of speed (b) as functions of the starting angle of a filament, obtained by simulations for $D_r T=0.12, 0.3, 0.6, 1.2, 3,$ and 6 rad^2 , where D_r is the rotational diffusion constant of the filament and T the tracking time.

may obtain a different speed. To get the distribution of the speed, the simulation was repeated 10 000 times for a given θ_0 , time interval T , and rotational diffusion constant D_r . The average speed and standard deviation were calculated from the 10 000 simulated speeds.

Figure 8 shows the average speed normalized by the value at 45° and its standard deviation as functions of the starting angle, calculated from the simulations for a filament with $D_r T=0.12, 0.3, 0.6, 1.2, 3,$ and 6 rad^2 . It is intuitive that the angular dependence of average speed and its standard deviation is stronger for a shorter tracking time and a smaller rotational diffusion coefficient. This angular dependence is weaker at larger $D_r T$ values. It is also interesting to note that the standard deviation increases with increasing $D_r T$ values, when $D_r T < 0.6 \text{ rad}^2$, and decreases after that.

According to Fig. 8, if we measure the speed of only one filament for a small $D_r T$ without knowing the starting angle, the error could be very large and the result is unreliable for calculating the mobility. One way to reduce the error is to increase the tracking time. However, the tracking time is restricted by the duration that the filament stays in the field of view. An alternative approach is to average the speed over several filaments. A simulation was made to obtain the average speed over a sample number of N_s filaments. To do this, we randomly choose a starting angle at $t=0$ and perform a round of simulation to get a speed for one value of $D_r T$. This process simulates a measurement of the speed of a filament during tracking time T . We repeat the simulation N_s times, much like measuring the speed of N_s randomly selected filaments. A speed is obtained by averaging over the N_s simulated speeds.

The above simulation is repeated 1000 times to obtain 1000 speeds, each averaged over N_s filaments of randomly selected starting angles. A normal distribution can be applied to these speeds (data not shown). The mean value of these

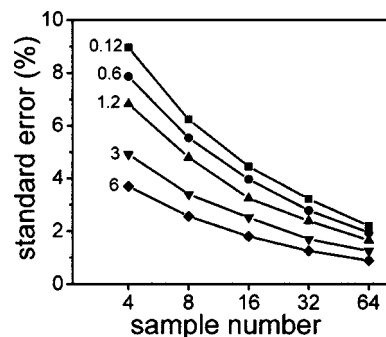


FIG. 9. Standard error of measured speed as a function of sample number, obtained by simulations for $D_r T=0.12, 0.6, 1.2, 3,$ and 6 rad^2 , where D_r is the rotational diffusion constant of F-actin and T the tracking time.

1000 speeds and the standard deviation of the mean (standard error) are calculated. The standard error is normalized by the mean and plotted as a function of the sample number for various $D_r T$ values, as shown in Fig. 9. As expected, the standard error decreases with increasing $D_r T$ and the sample number.

As a simple estimate, we assume that the F-actin measured is $3 \mu\text{m}$ long, of which the rotational diffusion coefficient is about $0.8 \text{ rad}^2/\text{s}$. So $D_r T \sim 2.4 \text{ rad}^2$. For a sample number of 16, the standard error is about 3%, estimated based on the data in Fig. 9. This means that if one measures a speed averaged over 16 randomly selected F-actin with 3 s tracking time, there is 95.4% probability that this speed is within 6% discrepancy of the real value, and 99.7% probability that it falls within 9% discrepancy of the real value. Rotational diffusion constant of fd virus is about $34 \text{ rad}^2/\text{s}$. A tracking time of 1 s is sufficient for fd virus with a sample number of 16. Therefore, our measurements are reliable based on these simulation results.

Rotational diffusion coefficient of a rod is proportional to L^{-3} . It increases quickly with decreasing rod length L . For very short filaments such as a DNA fragment, the rotational diffusion coefficient is very large. Thus the measured speed of a single molecule is reliable even by tracking a relatively short time, if the influence of translational diffusion is not important. However, for longer filaments, such as F-actin and microtubules, enough tracking time or sample number is required for a reliable measurement, which can be estimated directly from Fig. 9 for a rodlike molecule with known rotational diffusion constant.

V. SUMMARY

The orientation dependence of the drift speed of F-actin under an electric field is studied by single-molecule tracking in combination with fluorescence microscopy. Due to the anisotropy of hydrodynamic friction, a migrating actin filament shows an interesting dipping effect. The moving speed of F-actin depends on the angle between the filament axis and the electric field. This dependence is well described by the hydrodynamic theory of a rod in fluid. The influence of rotational diffusion on the electrophoretic mobility of F-actin is also measured. When the tracking time and the sample number are large enough, as chosen in our experiments, the standard error in mobility measurement is estimated to be less

than 3%. The mobility of F-actin in F-buffer is measured to be $-(8.5 \pm 0.7) \times 10^{-5} \text{ cm}^2/(\text{V s})$ when averaged over all orientations, by tracking 16 randomly selected F-actin filaments for over 3 s. We also show that the ratio between different macromolecules can be reliably determined. As an example, we obtain the mobility of fd virus in the F-actin buffer to be $-(1.07 \pm 0.09) \times 10^{-4} \text{ cm}^2/(\text{V s})$.

ACKNOWLEDGMENT

This work was supported by NSF under Grant Nos. DMR0320676, DMR0405156, and NIH R01 HL67286.

¹R. C. Allen, C. A. Saravis, and H. R. Maurer, *Gel Electrophoresis and Isoelectric Focusing of Proteins: Selected Techniques* (W. de Gruyter, Berlin, 1984).

²R. Kuhn and S. Hoffstetter-Kuhn, *Capillary Electrophoresis: Principles and Practice* (Springer, Berlin, 1993).

³E. Stellwagen and N. C. Stellwagen, *Electrophoresis* **23**, 2794 (2002).

⁴B. M. Paegel, C. A. Emrich, G. J. Wedemayer, J. R. Scherer, and R. A. Mathies, *Proc. Natl. Acad. Sci. U.S.A.* **99**, 574 (2002).

⁵D. A. Hoagland, E. Arvanitidou, and C. Welch, *Macromolecules* **32**, 6180 (1999).

⁶X. Feng and P. L. Dubin, *Langmuir* **18**, 2032 (2002).

⁷A. Castro and E. B. Shera, *Anal. Chem.* **67**, 3181 (1995).

⁸B. B. Haab and R. A. Mathies, *Anal. Chem.* **71**, 5137 (1999).

⁹M. R. Shortreed, H. Li, W.-H. Huang, and E. S. Yeung, *Anal. Chem.* **72**, 2879 (2000).

¹⁰E. S. Yeung, *Annu. Rev. Phys. Chem.* **55**, 97 (2004).

¹¹M. Doi and S. F. Edwards, *The Theory of Polymer Dynamics* (Oxford University Press, Oxford, 1988).

¹²W. Eimer and R. Pecora, *J. Chem. Phys.* **94**, 2324 (1991).

¹³J. Kas, H. Strey, J. Tang, D. Finger, R. Ezzell, E. Sackmann, and P. Janmey, *Biophys. J.* **70**, 609 (1996).

¹⁴A. J. Hunt, F. Gittes, and J. Howard, *Biophys. J.* **67**, 766 (1994).

¹⁵J. Sambrook, E. F. Fritsch, and T. Maniatis, *Molecular Cloning: A Laboratory Manual*, 2nd ed. (Cold Spring Harbor Laboratory, Plainview, New York, 1989).

¹⁶Q. Wen and J. X. Tang, *J. Chem. Phys.* **121**, 12666 (2004).

¹⁷J. Horvath and V. Dolnik, *Electrophoresis* **22**, 644 (2001).

¹⁸M. Gillges, M. H. Kleemlss, and G. Schomburg, *Anal. Chem.* **66**, 2038 (1994).

¹⁹D. Belder, A. Deege, H. Husmann, F. Kohler, and M. Ludwig, *Electrophoresis* **22**, 3813 (2001).

²⁰G. Li and J. Tang, *Phys. Rev. E* **69**, 061921 (2004).

²¹S. Broersma, *J. Chem. Phys.* **74**, 6989 (1981).

²²M. M. Tirado and J. d. I. Torre, *J. Chem. Phys.* **71**, 2581 (1979).

²³M. M. Tirado, C. L. Martínez, and J. G. d. I. Torre, *J. Chem. Phys.* **81**, 2047 (1984).

²⁴H. Qian, M. P. Sheetz, and E. L. Elson, *Biophys. J.* **60**, 910 (1991).